electronics

MDPI

Article

Enhancing Image Clarity: A Non-Local Self-Similarity Prior Approach for a Robust Dehazing Algorithm

Wujing Li [1,2], Yuze Liu [1], Xianfeng Ou [1,2], Jianhui Wu [1,2] and Longyuan Guo [1,2,*]

1 School of Information and Communication Engineering, Hunan Institute of Science and Technology, Yueyang 414006, China; liwj@hnist.edu.cn (W.L.)
2 Machine Vision & Artificial Intelligence Research Center, Hunan Institute of Science and Technology, Yueyang 414006, China
* Correspondence: guolongyuan@hnist.edu.cn

Abstract: When light propagates in foggy weather, it is affected and scattered by suspended particles in the air. As a result, images taken in this environment often suffer from blurring, reduced contrast, loss of details, and other issues. The primary challenge in dehazing images is to estimate the transmission coefficient map in the atmospheric degradation model. In this paper, we propose a dehazing algorithm based on the optimization of the "haze-line" prior and non-local self-similarity prior. First, we divided the input haze image into small blocks and used the nearest neighbor classification algorithm to cluster the small patches, which were referred to as "patch-lines". Based on the characteristics of these "patch-lines", we could estimate the transmission coefficient map for the image. We then applied the transmission map to a weighted least squares filter to smooth it. Finally, we calculated the clear image using the haze degradation model. The experimental results demonstrate that our algorithm enhanced the image contrast and preserved the fine details, both qualitatively and quantitatively.

Keywords: image dehazing; non-local self-similarity prior; nearest neighbor classification

check for updates

Citation: Li, W.; Liu, Y.; Ou, X.; Wu, J.; Guo, L. Enhancing Image Clarity: A Non-Local Self-Similarity Prior Approach for a Robust Dehazing Algorithm. *Electronics* **2023**, *12*, 3693. https://doi.org/10.3390/electronics12173693

Academic Editor: Silvia Liberata Ullo

Received: 3 August 2023
Revised: 30 August 2023
Accepted: 30 August 2023
Published: 31 August 2023

1. Introduction

Haze is a common weather phenomenon caused by a large number of small particles or suspended water droplets in the atmosphere. In hazy conditions, light is scattered and refracted by these particles and droplets, resulting in reduced contrast, loss of detail, and degraded image quality in outdoor scenes [1]. These effects can seriously impact the application of outdoor computer vision systems, such as road monitoring, environmental monitoring, and remote sensing [2].

Recently, single-image recovery algorithms have made significant progress [3–8]. Based on prior knowledge, image restoration algorithms invert the degradation process and compensate for image distortion to obtain a clear image. However, estimating the depth information of the image scene and atmospheric light value remains challenging. In recent years, Berman [8] and others proposed a non-local dehazing algorithm based on the "haze-line" prior. In hazy images, pixels at varying depths are impacted to different degrees. Pixels that originally shared the same values no longer cluster together in the RGB space after being affected; instead, they disperse along a line known as the "haze line". It is an excellent algorithm that can restore a clear image, but its single-pixel-based approach has weak robustness.

In this work, we propose a single image dehazing algorithm based on a non-local self-similarity prior. The self-similarity prior in natural images shows that a local patch often has many non-local similar patches, and has been widely used in many image processing tasks. We improved upon the "haze-line" prior-based algorithm by using the non-local self-similarity prior to achieve the goal of optimizing the original algorithm. The contributions of this work are summarized as follows:

(1) Enhanced non-local self-similar prior: This innovation lies in the replacement of the traditional single-pixel-based non-local prior knowledge with an advanced approach based on image self-similarity. This shift results in improved robustness, and better restoration of natural images.
(2) Similarity metric for patch clustering: This paper introduces a novel method to measure the similarity of hazy patches, enabling more accurate clustering of small patches. This innovation contributes to refining the accuracy of estimating scene transmission and atmospheric light values.

The remainder of this paper is organized as follows: Section 2 reviews the degradation model and related work, and Section 3 provides a detailed explanation of the proposed algorithm. Section 4 presents the results and comparisons with other algorithms, and Section 5 concludes the proposed algorithm and discusses future work.

2. Related Work

2.1. Haze Image Degradation Model

In a hazy environment, the quality of object imaging is significantly reduced due to the influence of suspended particles in the atmosphere on light transmission and reflection. Based on the theory of atmospheric scattering, the scattering of light by small particles in the atmosphere can be divided into two components: one is the attenuation of reflected light from the object's surface to the camera due to the medium in the air, and the other is the additional hazy light from light scattered by particles in the air between the camera and the scene. To account for this phenomenon, Narasimhan [9] proposed the atmospheric scattering model:

$$I(x,y) = J(x,y)t(x,y) + A[1 - t(x,y)] \tag{1}$$

In Equation (1), $I(x,y)$ represents the hazy image captured in outdoor scenes, which has reduced contrast and degraded colors. $J(x,y)$ denotes the dehazed image, also known as the clear image. A is the airlight, or the intensity of the light that has been scattered by the atmosphere before reaching the camera. Meanwhile, $t(x,y)$ represents the transmission coefficient, which indicates the portion of light reaching the camera, and the value lies between 0 and 1. The larger the transmission coefficient, the lower the contribution from the airlight term and the lower the loss of light. When the atmosphere is homogenous, $t(x,y)$ can be expressed as

$$t(x,y) = \exp(-\theta d(x,y)) \tag{2}$$

In Equation (2), θ represents the atmospheric scattering coefficient, which is commonly considered a constant. The variable $d(x,y)$ denotes the distance between the object in the image and the imaging device, or in other words, the depth of the scene. Typically, it is assumed that the values of the three color channels are equivalent. As the distance between the object and the device increases, the transmission coefficient is expected to decrease, resulting in a more blurred image. Given the known hazy image $I(x,y)$, it is challenging to solve for other unknown parameters, such as the airlight and transmission coefficients using Equation (1) to obtain the target image $J(x,y)$. This equation does not have a solution and requires a prior constraint to solve.

2.2. Overview of the Single-Image Dehazing Algorithm

Single-image dehazing algorithms aim to improve the visibility and quality of hazy images without relying on multiple input images or depth information. At present, the existing image dehazing methods can be mainly divided into three categories: image enhancement, image restoration, and deep learning methods.

Image enhancement methods mainly focus on improving the visual effect and improving the visibility of the image by adjusting parameters such as the image contrast, brightness, and color balance. These methods generally do not involve the image degradation model, but instead start from a visual perspective, aiming to improve the image's appearance. For example, the Retinex model [10,11] is a classic image enhancement method that adjusts the brightness and contrast of an image, thereby enhancing the visual effect of the image. Without considering the spatial variance of the degradation, image enhancement methods tend to perform well in scenarios with uniform haze distribution, but the performance is unsatisfactory in scenes containing varying depths.

Image restoration methods are usually based on the image degradation model to recover clearer images by estimating the transmission coefficient and airlight to remove the effects of haze. The key to the methods lies in the estimation of parameters. In recent years, researchers proposed some priors, including the "haze-line" prior, to address this challenge. Fattal [6] estimated scene reflectivity based on prior knowledge that the transmission and surface shading are locally uncorrelated. While this method can provide a reliable transmission estimate, it does not perform well in dense fog images. To address this, He [7] and others proposed an image-dehazing method based on a dark channel prior and estimated the transmission coefficient through this prior knowledge. This algorithm achieves a good dehazing result but its complexity is high.

Deep learning [12,13] has been a hot research direction in recent years. These methods do not require an explicit image degradation model, but instead learn the complex features of images by training a neural network to achieve the dehazing effect. In the early algorithms, convolutional neural networks were predominantly employed to estimate the transmission coefficient in hazy images. Subsequently, the haze-free image was recovered based on the image degradation model. This type of haze removal algorithm is referred to as non-end-to-end image dehazing. Classic non-end-to-end image dehazing algorithms include DehazeNet [14] and AOD-net [15]. The most recent and widely adopted approach involves end-to-end image dehazing methods. In these methods, the network model takes hazy images as the input and generates haze-free images as the output. Notable examples of this approach include Clycle-Dehaze [16] and DehazeFormer [17]. The training process of the methods relies on an extensive dataset comprising real-world hazy images and their corresponding clear, haze-free counterparts. However, acquiring the datasets is challenging, and these methods might exhibit limitations in terms of interpretability and robustness.

2.3. Non-Local Self-Similarity Prior

Natural images contain a significant amount of self-similar information, which is a defining characteristic of images. Within the same image, image patches exhibit similar structural and textural details to other image patches, which is a phenomenon known as non-local self-similarity (NSS) [18]. NSS posits that multiple similar patches can be identified in different positions within a natural image. This prior has been leveraged in various computer vision applications, including image denoising and super-resolution. However, the presence of haze in images can disrupt the correlation of similar patches, leading to varying degrees of degradation, as illustrated in Figure 1.

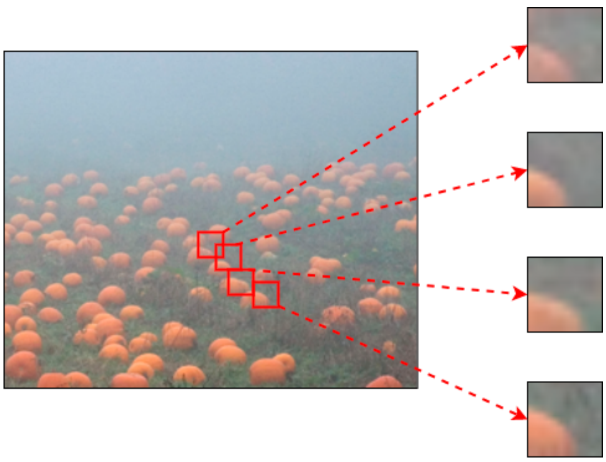

Figure 1. Example of similar patches in a degraded image.

Assuming that all degradation in the image is solely attributable to haze and not influenced by other factors, let us consider a set of small patches. In a natural image, this group of small patches should be identical. However, in a hazy image, their pixel values change due to varying scene depths. Let the pixel values of this set of similar small blocks be denoted as $P_1(x,y), P_2(x,y), \ldots, P_n(x,y)$. From Equation (1), we can observe that

$$P_n(x,y) = J(x,y)t_n(x,y) + A[1 - t_n(x,y)] \tag{3}$$

As the patches are small, we can assume that the depth remains constant within each patch. Thus, the value of $t(x)$ is the same across all small patches. Moreover, we assume that the atmospheric light in the small patches is uniform. From Equation (3), we can observe that the information within the small patches gradually deteriorates as the distance increases. Due to the impact of haze, the correlation between similar patches is linear in the RGB color space, meaning that

$$P_n(x,y) - A = (J(x,y) - A)t_n(x,y) \tag{4}$$

From Equation (4), we can observe that when $t_n(x,y) = 0$, $P_n(x,y) = A$; and when $t_n(x,y) = 1$, $P_n(x,y) = J(x,y)$. Therefore, the non-local self-similar prior knowledge can be applied to our image-dehazing algorithm. We can first identify small patches in hazy images that correspond to similar haze-free patches and cluster them into "patch-lines". As shown in Figure 1, the four enlarged patches represent self-similar scenes located at different distances in the image, and the closer image has less haze contribution than one further away. Together with other unlabeled similar patches, these patches are clustered into a "patch-line". Next, the two endpoints (the highest saturation and the lowest saturation) of the cluster can represent the original scene $J(x,y)$ and the airlight A, respectively.

3. Methodology

This section outlines our newly proposed dehazing algorithm, as shown in Figure 2. First, we divided the hazy images into small patches and preprocessed them due to the impact of haze before measuring their similarity. Second, we classified the small patches using the nearest neighbor classification method. Lastly, we performed error correction.

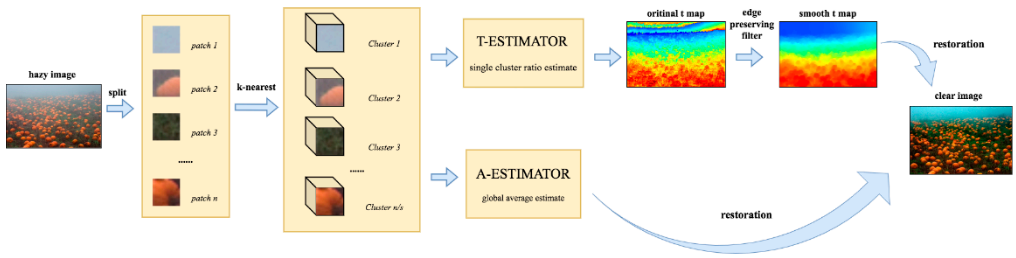

Figure 2. The flowchart of the proposed method.

After clustering the small patches into "patch-lines", we estimated the boundary values to determine the transmission coefficient $t(x,y)$ and atmospheric light A of the small patches. We then estimated the transmission coefficient map and smoothed it to carry out the dehazing process for the original hazy image.

3.1. Patch Segmentation and Preprocess

Many studies have used small patch segmentation to remove haze with various window sizes. For instance, He [7] used a 15×15 window in his method. To achieve optimal dehazing results, this study employed a small patch size of 4×4 and segmented the entire image.

As a result of the scattering effect of haze, originally similar small patches exhibit varying degrees of degradation. Consequently, measuring similarity using Euclidean distance alone is insufficient. New measurement standards must be established for degraded small patches, such as regularizing them before measuring similarity via Euclidean distance.

As shown in Equation (4) in Section 2.3, the relationship between a group of similar small patches is linear in the absence of airlight. Therefore,

$$\widetilde{P_n}(x,y) = \widetilde{J_n}(x,y)t_n(x,y) \tag{5}$$

The notation $\widetilde{P_n}(x,y)$ refers to the small patch obtained after removing the airlight component, while $\widetilde{J_n}(x,y)$ corresponds to the original image with the airlight component removed. According to Narasimhan [19], in areas where the color is uniform and the transmission coefficient $t(x,y)$ and airlight A in Equation (1) are locally uniform, we could eliminate the airlight component by subtracting the local average color. This elimination process is independent for each small patch, and is not affected by any differences in the airlight between patches.

$$\widetilde{P_n}(x,y) = P_n(x,y) - mean[P_n(x,y)] \tag{6}$$

$$\widetilde{J_n}(x,y) = J_n(x,y) - mean[J_n(x,y)] \tag{7}$$

Despite eliminating the airlight component, the effects of degradation caused by different depths are not uniform, and can still affect our ability to find similar small patches. To address this issue, we needed to regularize the small patches based on their norms in order to mitigate the influence of haze. The corresponding equation is as follows:

$$\| \widetilde{P_n}(x,y) \| = \| \widetilde{J_n}(x,y)t_n(x,y) \| = \| \widetilde{J_n}(x,y) \| \, t_n(x,y) \tag{8}$$

Based on Equation (8), we can conclude that a group of similar small patches will be equal to a fixed value as long as they are regularized. By continuing to use the Euclidean distance to measure the similarity of small patches, we can successfully classify them.

To prevent the nearest neighbor classification method from overfitting, we should select small patches with a large standard deviation. A threshold can be set as follows:

$$std\left(\widetilde{P_n}\right) \geq \eta, \eta = 0.01 \tag{9}$$

3.2. Nearest Neighbor Classification and Finding Boundary Patches

The KNN (k-nearest neighbor) algorithm is the simplest and most effective method for classifying the pre-treated patches. This algorithm is commonly used for classification purposes. Its core idea is that if most of the k nearest samples in the feature space belong to a certain category, then the sample being classified also belongs to that category. In other words, the category of a patch is determined by the category of its nearest neighbors [20]. To find the neighbors of small patches, we needed to measure the similarity between patches. The index we used for this purpose is the Euclidean distance. Patches with closer pixel values have smaller Euclidean distances and are considered to be more similar, as shown in Equation (10):

$$d\left(\widetilde{P_m}(x,y), \widetilde{P_n}(x,y)\right) = \sqrt{\sum_x \sum_y \left(\widetilde{P_m}(x,y) - \widetilde{P_n}(x,y)\right)^2} \tag{10}$$

Based on the calculated Euclidean distances, the small patches can be divided into k categories, where each category corresponds to a cluster of similar patches. In this study, we set the value of k to 100, which was sufficient to represent the different types of patches in the image. The aggregation of small patches is a crucial step in our method, as it directly affects the accuracy of the final estimation of the transmission coefficient map. The classification accuracy of small patches is especially important in this regard.

At this stage, we have gathered 100 clusters of similar patches. As described in Section 2.3, once we identified the boundary patch of each cluster, we could further estimate the transmission coefficient $t(x,y)$ and the airlight component A. Haze can greatly reduce the saturation of natural scenes in images [21]. To locate the boundary patch, we exploited this property by examining the saturation values of the patches within each cluster. Specifically, we identified the patches with the largest and smallest saturation values to estimate $t(x,y)$ and A, respectively. The saturation of small patches relative to the min–max values can be computed using the following equation:

$$S_p = \frac{\max_p(R,G,B) - \min_p(R,G,B)}{\max_p(R,G,B)} \tag{11}$$

In Equation (11), $\max_p(R,G,B)$ refers to the maximum value of the RGB channel among the pixels within a small patch, while $\min_p(R,G,B)$ refers to the minimum value of the RGB channel among the pixels within the same patch.

3.3. Estimate Transmission Coefficient and Airlight

Once we identified the patch clusters and located the patch with the highest saturation within each cluster, namely, the haze-free patch $J_n(x,y)$, we used this information to estimate $t(x)$ for each small patch by applying Equation (4). This approach enabled us to estimate an unknown quantity using two known quantities.

$$t_n(x,y) = \frac{P_n(x,y) - A}{J_n(x,y) - A} = \frac{\parallel \widetilde{P_n}(x,y) \parallel}{\parallel \widetilde{J_n}(x,y) \parallel} = \frac{std(P_n(x,y))}{std(J_n(x,y))} \tag{12}$$

Most algorithms assume that the airlight is uniform, and we also followed this assumption. Given that small patches within each patch cluster will degrade from a clear scene to a color similar to airlight, we estimated the airlight by identifying the boundary patch with the lowest saturation. To obtain an approximate value for the airlight of the entire image, we averaged the airlight value of all clusters. In this study, we did not assign equal weight to each boundary patch because a fewer number of blocks led to lower accuracy in estimating the airlight. The weight was assigned to each patch according to the size of the corresponding cluster. The cluster with a larger number of small patches was given a greater weight, whereas the cluster with fewer small patches was given a lower weight.

$$A = \sum \lambda_n \widetilde{A_n} / N \tag{13}$$

where λ_n represents the number of patches in the nth cluster, and N denotes the number of all patches.

3.4. Smooth Function

In Section 3.3, we obtained the $t(x,y)$ based on small patches, but it is evident that the resulting $t(x,y)$ was discontinuous and very rough. In actual scenes, the depth of field between adjacent pixels should be similar. Therefore, we also needed to smooth the depth map while maintaining the edge of the image object and making the image closer to reality. To achieve this, we used the weighted least squares filtering method, as shown in Equation (14):

$$\begin{aligned} \min\Phi\left(\hat{t}(x,y)\right) = \; & \sum_{x,y} \left(\hat{t}(x,y) - t(x,y)\right) \\ & + \omega \sum_x \sum_y \left(a_x \left(\tfrac{\partial \hat{t}(x,y)}{\partial x}\right)^2 + a_y \left(\tfrac{\partial \hat{t}(x,y)}{\partial y}\right)^2\right) \end{aligned} \tag{14}$$

In this equation, the first term represents the objective of making the input image and output image as similar as possible. The second term is a regularization term that encourages smoothness in the output image by minimizing the partial derivative, where a_x and a_y are weight coefficients. The parameter ω is employed to balance between the two terms, and the value was set to 0.05 in this study.

Even in sunny weather, there can still be a small number of suspended particles that affect the image. If all haze is completely removed, the resulting image may lose its sense of depth and appear distorted. Therefore, we chose to retain a portion of the haze to preserve the natural appearance of the image:

$$J(x,y) = \frac{I(x,y) - A}{\delta\, t(x,y)} + A \tag{15}$$

Here, δ is employed to adjust the amount of residual haze, and the value was set to 0.95 in this study.

4. Result

To validate the efficacy of our method, this section analyzes our experimental results both qualitatively and quantitatively, demonstrating the superiority of our new algorithm from multiple perspectives. In the experiments, we obtained the results of our algorithm and compared them with the results of other classical or recent dehazing algorithms, such as Berman [8], Ancuti C. O. [22], He [7], and Dhara S. K. [23]. The results of these dehazing algorithms were generated using the authors' codes and parameters. All experimental results were obtained using a PC equipped with a 1.6 GHz Intel Core i5 CPU and 4 GB memory and were implemented using MATLAB r2020a.

4.1. Qualitative Results

In the qualitative experiments, we performed comparisons on two separate datasets: the real outdoor hazy image dataset and the synthetic image dataset with a ground truth.

First, to intuitively compare the dehazing effects of different algorithms on real outdoor hazy images, we conducted numerous experiments on the classic foggy images in the Live Image Defogging image database [24]. This image database contains images captured by surveillance cameras, including various image types and different levels of haze density, with sizes ranging from 425 × 274 to 1024 × 768 pixels. Figure 3 presents the defogging results of several images in the dataset, including natural scenes, such as plants, soil, and trains. All five methods improved the quality of the hazy images. The first row shows that our algorithm could restore the clarity of heavily hazy forest areas. In the second row, our algorithm restored the scene's color more naturally. The third row demonstrates the restoration of a distant small train (located at the middle-left of the image) that was almost obscured by haze, revealing its original appearance. For the restoration of the fourth-row image, the color remained relatively natural, and the clarity was excellent. Berman's method fell short in removing dense fog in the image, as the color saturation in their dehazed images was excessive. Liu's method did not completely remove haze, and the result from He's method was not as clear as ours. Dhara S. K.'s method produced an apparent patching effect, resulting in an insufficiently smooth image. In contrast, our algorithm provided clear, high-definition, and low haze residue results, with excellent color restoration. The selected edge-preserving filter provided a higher gradient ratio, smoother edge details, and minimal blocking effect, making our dehazing algorithm highly effective.

Figure 4 shows the comparison of the recovery effect of our method with the ground truth on Fattal's hazy image database [6]. The dataset includes images with different densities of synthetic haze. The first column shows the original hazy images; the second and fourth columns display the dehazed images and transmission coefficients obtained through our method, respectively; and the third and fifth columns show the ground truth images and depth, respectively. It can be seen that our method could recover the clear details of the scenes and achieve a high degree of haze removal. The edge boundaries of our dehazed images were also very clear, and the estimation of the close-range depth of field was relatively accurate. However, some notable errors in the transmission coefficient maps can be observed. These errors stemmed from mismatched positions within the haze line, incorrect clustering, and other factors. For instance, some areas exhibited significantly high brightness values with low saturation, which were similar to those of the airlight, consequently leading to underestimated transmission coefficient values compared with the ground truth, such as the white wall in the upper right corner in 'Church', the windows in 'Mansion', the person's face in the middle in 'Raindeer', and the left part of the big stone at the bottom in 'Road1'. This phenomenon requires further study.

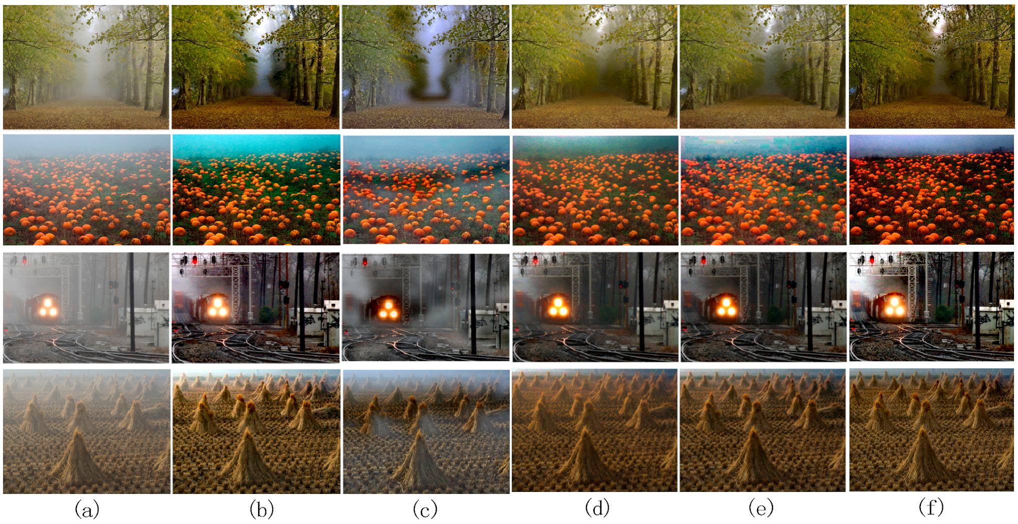

Figure 3. The dehazing results: (**a**) the blurred image of nature in the database; (**b**) the restoration result of Berman; (**c**) the recovery result of Ancuti C. O.; (**d**) the recovery result of He; (**e**) the recovery result of Dhara S. K.; (**f**) the recovery result of our method.

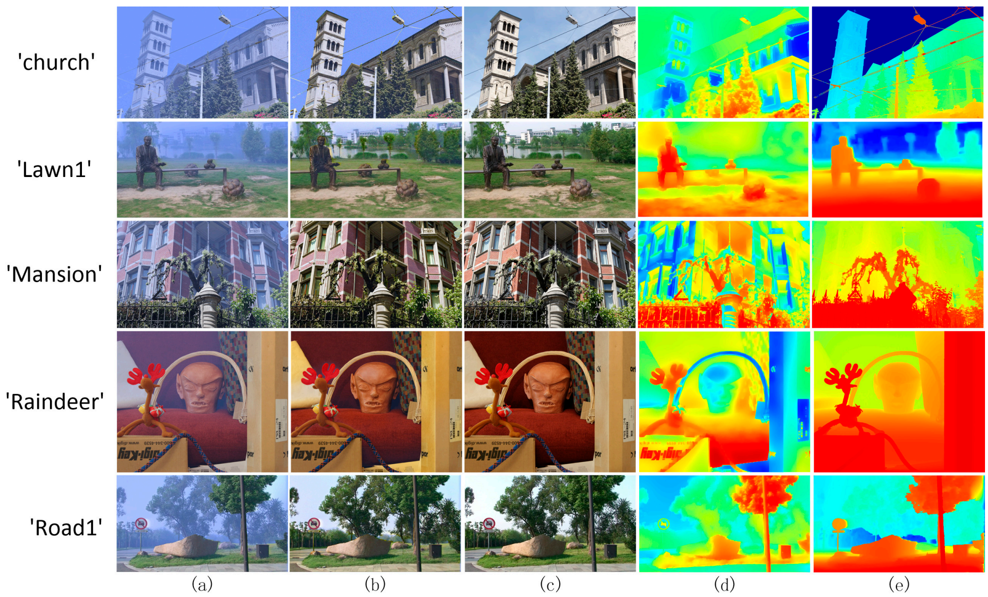

Figure 4. The restoration of hazy images in Fattal's database using our dehazing method: (**a**) the natural scene image with synthetic haze; (**b**) a dehazed image recovered using our algorithm; (**c**) the clear image provided by the database; (**d**) the transmission coefficient map recovered by our method; (**e**) the true depth of a scene provided by the database.

4.2. Quantitative Results

To objectively evaluate the effectiveness of our algorithm, we used the natural scene synthetic haze image dataset with haze-free images of Fattal, as shown in Figure 4. The same distribution of zero-mean Gaussian noise was added to the test haze images at three different noise levels: σ =0.01, 0.025, and 0.5. We employed the L1 error calculation method to quantitatively evaluate the experimental results and compared them with those of the classical dehazing algorithm. According to the definition of the L1 error, the smaller the error value, the closer the image is to the haze-free image, and the better the image dehazing method it represents.

Our algorithm was compared with some other classical algorithms and the results are shown in Table 1. The numbers are given as X/Y, where X records the L1 error of the transmission coefficient, while Y records the L1 error of the dehazed image.

Table 1. L1 error result data comparison of each algorithm.

Image	σ	Berman [8]	He [7]	Ours
Church	0	0.047/0.032	0.039/0.025	0.115/0.075
	0.01	0.049/0.041	0.053/0.043	0.085/0.063
	0.025	0.047/0.057	0.089/0.081	0.082/0.065
	0.05	0.043/0.092	0.121/0.136	0.083/0.074
Lawn1	0	0.032/0.026	0.077/0.035	0.040/0.030
	0.01	0.032/0.032	0.056/0.038	0.038/0.031
	0.025	0.052/0.056	0.056/0.065	0.037/0.036
	0.05	0.099/0.107	0.113/0.121	0.033/0.047
Mansion	0	0.080/0.049	0.042/0.022	0.065/0.053
	0.01	0.088/0.056	0.048/0.030	0.066/0.055
	0.025	0.104/0.072	0.065/0.051	0.066/0.057
	0.05	0.116/0.095	0.081/0.080	0.069/0.065
Raindeer	0	0.089/0.045	0.066/0.034	0.070/0.039
	0.01	0.093/0.049	0.077/0.042	0.069/0.039
	0.025	0.104/0.063	0.084/0.054	0.067/0.041
	0.05	0.131/0.092	0.106/0.083	0.066/0.045
Road1	0	0.058/0.040	0.069/0.033	0.040/0.035
	0.01	0.061/0.045	0.068/0.038	0.048/0.038
	0.025	0.072/0/064	0.084/0.065	0.046/0.042
	0.05	0.092/0.100	0.120/0.114	0.044/0.051

It can be seen from Table 1 that the errors and relative distortion of most of the images in the data set of our algorithm were small. The performance of our algorithm was great and reached the current leading level. The experimental results show that our algorithm can deal with noise well. We found that our method is superior to other classical methods in terms of indicators for any noise level of low, middle, or high. However, with the increase in noise, the recovery effect of our method will decline.

5. Conclusions

In this paper, we propose an image dehazing algorithm based on non-local self-similarity prior. Enhanced non-local self-similar prior and similarity metrics for patch clustering are introduced in the algorithm. First, we divided the input haze image into small patches. Second, the nearest neighbor classification algorithm was employed to cluster small patches. Then, the transmission coefficient map and the airlight were estimated based on the non-local self-similarity prior. Finally, the final dehazing image was calculated.

In the experiment section, we performed image quality evaluation to test the image dehazing effects on the real outdoor hazy image dataset, and the synthetic image dataset with the ground truth. Compared with other methods, the proposed method has better performance on visual effects and quality evaluation indicators.

However, our algorithm has some limitations that need to be improved. First, the transmission coefficient may be estimated incorrectly in some cases, such as a missing haze-free patch in the cluster and insufficient color information with low saturation. Second, the haze image degradation model may be invalid. In addition, the efficiency of the algorithm needs to be improved to meet the requirements of real-time processing. In the future, we will conduct research on real-time and more complex models.

Author Contributions: Supervision, L.G.; writing—original draft, W.L. and Y.L.; writing—review and editing, J.W. and X.O. All authors have read and agreed to the published version of the manuscript.

Funding: This research was funded by the Hunan Provincial Natural Science Foundation, grant number 2020JJ5218, and by the Scientific Research Fund of the Education Department of Hunan Province, grant number 18B345.

Data Availability Statement: Not applicable.

Conflicts of Interest: The authors declare no conflict of interest.

References

1. Li, Y.; You, S.; Brown, M.S.; Tan, R.T. Haze Visibility Enhancement: A Survey and Quantitative Benchmarking. *Comput. Vis. Image Underst.* **2017**, *165*, 1–16. [CrossRef]
2. Shwartz, S.; Namer, E.; Schechner, Y.Y. Blind Haze Separation. In Proceedings of the 2006 IEEE Computer Society Conference on Computer Vision and Pattern Recognition (CVPR'06), New York, NY, USA, 16–22 June 2006; IEEE: Piscataway, NJ, USA, 2006; Volume 2.
3. Li, P.; Tian, J.; Tang, Y.; Wang, G.; Wu, C. Deep Retinex Network for Single Image Dehazing. *IEEE Trans. Image Process.* **2021**, *30*, 1100–1115. [CrossRef]
4. Tan, R.T. Visibility in Bad Weather from a Single Image. In Proceedings of the 2008 IEEE Conference on Computer Vision and Pattern Recognition, Anchorage, AK, USA, 23–28 June 2008; IEEE: Piscataway, NJ, USA, 2008.
5. Kim, J.H.; Jang, W.D.; Sim, J.Y.; Kim, C.S. Optimized contrast enhancement for real-time image and video dehazing. *J. Vis. Commun. Image Represent.* **2013**, *24*, 410–425. [CrossRef]
6. Fattal, R. Dehazing Using Color-Lines. *ACM Trans. Graph.* **2014**, *34*, 1–14. [CrossRef]
7. He, K.; Sun, J.; Tang, X. Single Image Haze Removal Using Dark Channel Prior. In Proceedings of the 2009 IEEE Conference on Computer Vision and Pattern Recognition, Miami, FL, USA, 20–25 June 2009; IEEE: Piscataway, NJ, USA, 2009.
8. Berman, D.; Treibitz, T.; Avidan, S. Non-Local Image Dehazing. In Proceedings of the 2016 IEEE Conference on Computer Vision and Pattern Recognition (CVPR), Las Vegas, NV, USA, 26 June–1 July 2016; IEEE: Piscataway, NJ, USA, 2016.
9. Narasimhan, S.G.; Nayar, S.K. Vision and the Atmosphere. *Int. J. Comput. Vis.* **2002**, *48*, 233–254. [CrossRef]
10. Land, E.H.; McCann, J.J. Lightness and Retinex Theory. *J. Opt. Soc. Am.* **1971**, *61*, 1. [CrossRef] [PubMed]
11. Liu, M.; Chen, J.; Han, X. Research on Retinex Algorithm Combining with Attention Mechanism for Image Enhancement. *Electronics* **2022**, *11*, 3695. [CrossRef]
12. Dong, S.; Wang, P.; Abbas, K. A Survey on Deep Learning and Its Applications. *Comput. Sci. Rev.* **2021**, *40*, 100379. [CrossRef]
13. Alom, M.Z.; Taha, T.M.; Yakopcic, C.; Westberg, S.; Sidike, P.; Nasrin, M.S.; Hasan, M.; Van Essen, B.C.; Awwal, A.A.S.; Asari, V.K. A State-of-the-Art Survey on Deep Learning Theory and Architectures. *Electronics* **2019**, *8*, 292. [CrossRef]
14. Cai, B.; Xu, X.; Jia, K.; Qing, C.; Tao, D. DehazeNet: An End-to-End System for Single Image Haze Removal. *IEEE Trans. Image Process.* **2016**, *25*, 5187–5198. [CrossRef] [PubMed]
15. Li, B.; Peng, X.; Wang, Z.; Xu, J.; Feng, D. AOD-Net: All-in-One Dehazing Network. In Proceedings of the 2017 IEEE International Conference on Computer Vision (ICCV), Venice, Italy, 22–29 October 2017; IEEE: Piscataway, NJ, USA, 2017.
16. Engin, D.; Genc, A.; Ekenel, H.K. Cycle-Dehaze: Enhanced CycleGAN for Single Image Dehazing. In Proceedings of the 2018 IEEE/CVF Conference on Computer Vision and Pattern Recognition Workshops (CVPRW), Salt Lake City, UT, USA, 18–22 June 2018; IEEE: Piscataway, NJ, USA, 2018.
17. Song, Y.; He, Z.; Qian, H.; Du, X. Vision Transformers for Single Image Dehazing. *IEEE Trans. Image Process.* **2023**, *32*, 1927–1941. [CrossRef] [PubMed]
18. Bahat, Y.; Irani, M. Blind Dehazing Using Internal Patch Recurrence. In Proceedings of the 2016 IEEE International Conference on Computational Photography (ICCP), Evanston, IL, USA, 13–15 May 2016; IEEE: Piscataway, NJ, USA, 2016.
19. Narasimhan, S.G.; Nayar, S.K. Contrast Restoration of Weather Degraded Images. In Proceedings of the ACM SIGGRAPH ASIA 2008 Courses on—SIGGRAPH Asia' 08, Singapore, 10–13 December 2008; ACM Press: New York, NY, USA, 2008.
20. Lee, J.M. An Efficient kNN Algorithm. *KIPS Trans. Part B* **2004**, *11*, 849–854. [CrossRef]
21. Zhu, Q.; Mai, J.; Shao, L. A Fast Single Image Haze Removal Algorithm Using Color Attenuation Prior. *IEEE Trans. Image Process.* **2015**, *24*, 3522–3533. [CrossRef] [PubMed]
22. Ancuti, C.O.; Ancuti, C. Single Image Dehazing by Multi-Scale Fusion. *IEEE Trans. Image Process.* **2013**, *22*, 3271–3282. [CrossRef] [PubMed]

23. Dhara, S.K.; Roy, M.; Sen, D.; Kumar Biswas, P. Color Cast Dependent Image Dehazing via Adaptive Airlight Refinement and Non-Linear Color Balancing. *IEEE Trans. Circuits Syst. Video Technol.* **2021**, *31*, 2076–2081. [CrossRef]
24. LIVE Image Defogging Database. Available online: http://live.ece.utexas.edu/research/fog/fade_defade.html (accessed on 10 August 2022).